Motion compensation for ISAR based on the shift-and-convolution algorithm

Conference Paper · May 2006

DOI: 10.1109/RADAR.2006.1631825 · Source: IEEE Xplore

Alvaro Blanco del Campo
Delft University of Technology

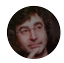

Alberto Asensio
Universidad Politécnica de Madrid

B.P. Dorta-Naranjo
Universidad de Las Palmas de Gran Canaria

Motion Compensation for ISAR based on the Shift-and-Convolution Algorithm

J.M. Muñoz-Ferreras, J. Calvo-Gallego, F. Pérez-Martínez, A. Blanco-del-Campo, A. Asensio-López
Departamento de Señales, Sistemas y Radiocomunicaciones
Universidad Politécnica de Madrid
Madrid, Spain
jmmunoz@gmr.ssr.upm.es, jaime@gmr.ssr.upm.es, felix@gmr.ssr.upm.es, alvaro@gmr.ssr.upm.es, vera@gmr.ssr.upm.es

B.P. Dorta-Naranjo
Departamento de Señales y Comunicaciones
Universidad Las Palmas de Gran Canaria
Las Palmas de Gran Canaria, Spain
pdorta@dsc.ulpgc.es

***Abstract*— ISAR (Inverse Synthetic Aperture Radar) is a coherent technique that obtains images of targets by processing the echoes returned during the dwell time. A higher angular resolution than the antenna beamwidth may be obtained. In this paper we report high resolution ISAR images, which have been obtained from data captured by a millimeter-wave LFMCW (Linear Frequency Modulated Continuous Wave) radar. The target translational motion compensation is achieved by means of a new parametric algorithm, which makes use of the shift-and-convolution technique. This image autofocusing algorithm is compared with Prominent Point Processing (PPP) and Phase Gradient Autofocus (PGA). Simulated and real data from the millimeter-wave LFMCW radar are used to verify the proposed technique, although the method is also applicable to any kind of coherent radar.**

I. Introduction

In conventional ISAR imaging, a high range resolution coherent radar remains static, illuminating a scene with a unique mobile target, from which an image is to be obtained [1]. It is necessary to collect several range profiles in order to obtain the cross-range information. Those parts of the target which have different radial velocities with respect to the radar position will be distinguished, as long as the Doppler gradient is greater than the Doppler resolution [2].

The range resolution improves with the increase of the transmitted bandwidth, while the cross range resolution is higher when the aspect angle change of the target during the Coherent Processing Interval (CPI) is greater. The range and cross range resolutions are given by the following two expressions:

$$\rho_{\mathrm{r}} = \frac{c}{2 \cdot B} \tag{1}$$

$$\rho_{\mathrm{a}} = \frac{\lambda}{2 \cdot \theta_{\mathrm{t}}}, \tag{2}$$

where c is the light speed, B is the transmitted bandwidth, λ is the wavelength and θ_{t} is the aspect angle change of the target during the CPI.

The type and quality of the final ISAR images depend strongly on the target motion. For example, if there is no Doppler gradient among the scatterers situated in the same range cell, it is not possible to obtain the second dimension (cross range) in the ISAR image. Moreover, as it is well known, the target view obtained in the ISAR image depends on the direction of the effective rotation vector. If the direction of this vector changes during the CPI, the ISAR image corresponds to a combination of different views, what complicates the interpretation of the result and indicates tridimensional information [3].

The real targets are engaged in complicated maneuvers, but the target motion is generally divided in translational and rotational components. The rotational component is the desired one, since it is the responsible of the generation of the Doppler gradient among the target scatterers. Nevertheless, it can also cause blurring effects: the MTRC (Migration Through Resolution Cells) [4]. In this paper we deal not with the MTRC. We concentrate on the translational motion compensation.

The radial component (LOS projection) of the translational motion is responsible of extreme blurring in the ISAR images and, therefore, it must be compensated in order to generate focused images. The blurring artifacts happen not only in range but also in cross range. The ones in range are caused by the change in range of the scatterers during the slow time, while the cause of the cross range blurring artifacts is the fact that the effective dwell time is reduced because of the scatterer migration.

The traditional methods solve the translational motion compensation problem in two steps: range-bin alignment and phase adjustment. The first step can be achieved by locking the first strong peak or by other techniques such as envelope correlation or spectral domain phase difference [1]. Exponentially averaged envelope correlation [5], minimum-entropy method [6], Hough Transform based method [7] and global range alignment [8] are other approaches found in the literature. In the second step, there are various schemes, such as PPP [9], PGA [10], entropy minimization method [11] and contrast maximization technique [12].

In this paper a different method for translational motion compensation is presented. It is also shown a data model for LFMCW radar in order to generate simulated data. Finally, the proposed technique is compared with PPP and PGA for simulated and real data.

II. Data Model

The real data used in this paper were captured by a high down-range resolution millimeter-wave LFMCW radar. This kind of radar is becoming more common compared to pulsed radars, because of the Low Probability of Interception associated with this waveform together with the lower peak power required for the same range.

The mathematical development here is similar to that in [13], where a chirped pulsed radar is assumed. In this paper, it is considered that the transmitted signal is a continuous carrier which is frequency modulated using a sawteeth signal. Fig. 1 shows the signal parameters. Δf is the emitted bandwidth and T_m is the period.

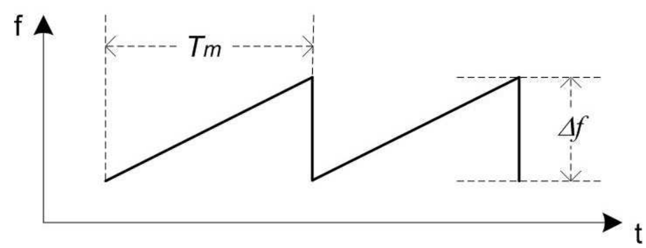

Fig. 1. Transmitted waveform

The following model, in complex envelope form, is assumed for the transmitted signal for a period T_m:

$$s_\mathrm{T}(t) = \exp\left[j\left(\omega_0 t + \pi\gamma\hat{t}^2\right)\right], \tag{3}$$

where ω_0 is the carrier pulsation, γ is the frequency modulation rate and $\hat{t}$ is the fast time, i.e. $\hat{t} = t - \mathrm{m}T_\mathrm{m}$ being m the ramp number. The frequency modulation rate γ is given by (4), according to Fig. 1.

$$\gamma = \frac{\Delta f}{T_\mathrm{m}}. \tag{4}$$

The received signal due to the i-th scatterer of the target is

$$s_{R_\mathrm{i}}(t) = a_\mathrm{i} \cdot \exp\left[j\left(\omega_0\left(t - t_{R_\mathrm{i}}\right) + \pi\gamma\left(\hat{t} - t_{R_\mathrm{i}}\right)^2\right)\right], \tag{5}$$

where a_i is the complex amplitude of the scatterer and t_{R_i} is the round trip time:

$$t_{R_\mathrm{i}} = \frac{2 \cdot R_\mathrm{i}}{c}, \tag{6}$$

being c the light speed and R_i the position of the i-th scatterer with respect to the radar.

We consider the stop-and-go assumption, i.e. R_i varies only with the slow time according to the target dynamics.

A sample of the transmitted signal (3) is used for the deramping process in the LFMCW radars. The deramped output signal for the i-th scatterer is

$$\begin{aligned}\widetilde{x}_{\mathrm{O_i}}(t) &= s_\mathrm{T}(t) \cdot s^*_{R_\mathrm{i}}(t) \\ &= a_\mathrm{i} \exp\left[j\left(\frac{4\pi\Delta f R_\mathrm{i}}{cT_\mathrm{m}}\hat{t} + \frac{4\pi f_0 R_\mathrm{i}}{c} + RVP\right)\right],\end{aligned} \tag{7}$$

where RVP is the Residual Video Phase, which is given by (8) and can be neglected [13].

$$RVP = -\frac{4\pi\Delta f R_\mathrm{i}^2}{T_\mathrm{m} c^2}. \tag{8}$$

According to (7), the scatterer range information is in the frequency domain. There is a linear relationship between range and frequency (usually called beat frequency, f_b):

$$R = \frac{c f_\mathrm{b} T_\mathrm{m}}{2\Delta f} \tag{9}$$

The final data model is the coherent sum of (7) for all the Q scatterers which compose the target:

$$\widetilde{x}_\mathrm{O}(t) = \sum_{\mathrm{i}=1}^{Q} a_\mathrm{i} \exp\left[j\left(\frac{4\pi\Delta f R_\mathrm{i}}{cT_\mathrm{m}}\hat{t} + \frac{4\pi f_0 R_\mathrm{i}}{c} + RVP\right)\right]. \tag{10}$$

This is the model assumed to generate simulated data, which are used to verify the motion compensation technique.

III. Motion Compensation Technique

The proposed method works on a single step and is parametric, unlike PPP and PGA. The technique makes use of the shift-and-convolution algorithm [14], which achieves a very accurate estimation of the centroid of a signal and has been applied successfully in the measurement of range and azimuth of extended targets.

In this case the consecutive range profiles are the signals to be processed. The generic scheme of the shift-and-convolution algorithm is shown in Fig. 2. The objective is to obtain the centroid of the target accurately in each range profile, so that the radial translational speed and acceleration of the target can be estimated during the dwell time, i.e. the coherent processing interval. For each range profile, the samples are convoluted with delayed and forwarded versions of the input signal (called the 'late' and the 'early' signal, respectively). The sum (Σ) and difference (Δ) of the low-pass filtered 'late' and 'early' signals are formed. The signal Δ/Σ is then constructed. The zero-crossing point of Δ/Σ gives information of the centroid position, a zero-crossing detector being used to compute it. Subsequently, a linear function is interpolated between the two adjacent samples to the zero-crossing point. The technique has no quantization error, in comparison with other alternatives. Moreover, theoretical and experimental results prove that the technique works correctly in noisy scenarios.

The proposed motion compensation technique is described in the following steps and its flowchart is shown in Fig. 3:

- *Step 1.* Let $\mathbf{M}_\mathrm{I}(\mathrm{m}, \mathrm{n})$ be the initial matrix, an M-by-N 2-D complex data matrix, where M is the number of

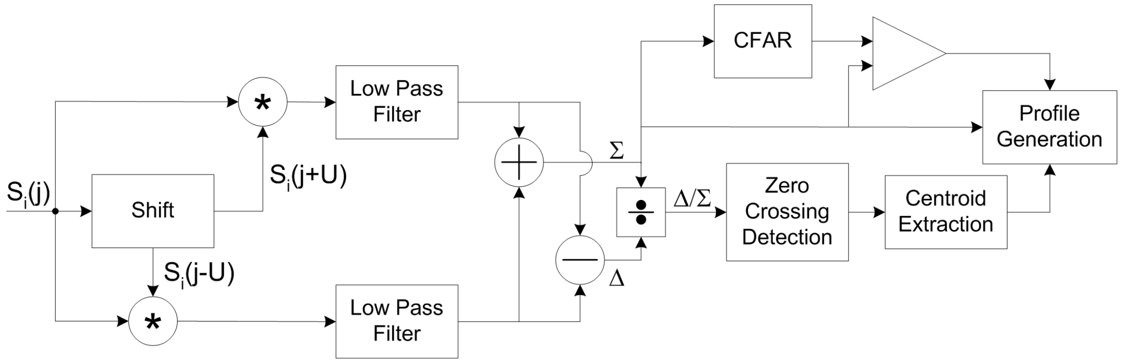

Fig. 2. Shift-and-convolution algorithm scheme

range profiles and N is the number of range cells. Therefore, $\mathbf{M}_{\mathrm{I}}(\mathrm{m},\mathrm{n})$ is compressed in range. Compute the centroid of each range profile by means of the shift-and-convolution algorithm. Subsequently, construct the centroid temporal evolution.

- *Step 2*. Estimate the target radial translational velocity (v_{e}) and acceleration (a_{e}), by means of adjusting a parabolic curve to the centroid temporal evolution.

- *Step 3*. Calculate the 'migrated range' $(\Omega_{\mathrm{i}}, \mathrm{i} = 0, 1, ..., M-1)$ for each profile with respect to the first, according to the next expression, where PRF is the pulse repetition rate and ΔR is the range resolution:

$$\Omega_{\mathrm{i}} = \frac{2\pi}{N}\frac{v_{\mathrm{e}}\mathrm{i}\dfrac{1}{PRF} + \dfrac{1}{2}a_{\mathrm{e}}\left(i\dfrac{1}{PRF}\right)^2}{\Delta R} \tag{11}$$

- *Step 4*. Perform a range decompression as an N-point Inverse Discrete Fourier Transform (IDFT) for each of the M range profiles, to generate $\mathbf{M}_{\mathrm{IDFT}}(\mathrm{m},\mathrm{n})$, i.e.,

$$\mathbf{M}_{\mathrm{IDFT}}(\mathrm{m},\mathrm{n}) = \mathrm{IDFT}_{\mathrm{n}}\{\mathbf{M}_{\mathrm{I}}(\mathrm{m},\mathrm{n})\} \tag{12}$$

- *Step 5*. Multiply each $\mathbf{M}_{\mathrm{IDFT}}(\mathrm{m},\mathrm{n})$ row by the complex exponential associated with the 'migrated range' Ω_{i}, obtaining $\mathbf{M}_{\mathrm{CIDFT}}(\mathrm{m},\mathrm{n})$ as a result, i.e. apply (13), where $\mathbf{n} = [0, 1, ..., N-1]$.

$$\begin{gathered}\mathrm{row}_{\mathrm{i}}\{\mathbf{M}_{\mathrm{CIDFT}}(\mathrm{m},\mathrm{n})\} = \\ \mathrm{row}_{\mathrm{i}}\{\mathbf{M}_{\mathrm{IDFT}}(\mathrm{m},\mathrm{n})\} \cdot \exp\left(j\Omega_{\mathrm{i}}\mathbf{n}\right), \\ \mathrm{i} = 0, 1, ..., M-1\end{gathered} \tag{13}$$

- *Step 6*. Generate the ISAR image, performing a 2D-Discrete Fourier Transform on $\mathbf{M}_{\mathrm{CIDFT}}(\mathrm{m},\mathrm{n})$ and taking the absolute value:

$$\mathbf{I}(\mathrm{m},\mathrm{n}) = |2\mathrm{D}-\mathrm{DFT}_{\mathrm{m,n}}\{\mathbf{M}_{\mathrm{CIDFT}}(\mathrm{m},\mathrm{n})\}| \tag{14}$$

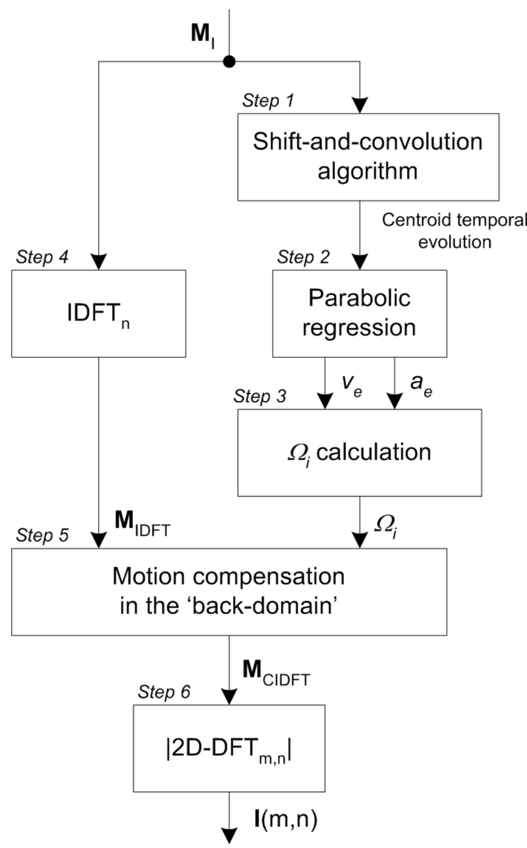

Fig. 3. Flowchart of the proposed technique

We rely on the high accuracy of the shift-and-convolution algorithm in the measurement of the centroid position to correctly compensate the translational motion. A novel idea with respect to other algorithms is to achieve the motion compensation in the 'back-domain' (Steps 5 and 6).

IV. Results

The obtained results shown in this section are compared with PPP and PGA. References [9] and [10] describe these techniques properly. An extension of envelope correlation has been used in these comparisons for the coarse range-bin alignment. In this extension the m-th reference envelope $(R_{\mathrm{m}}(\mathrm{n}))$ for the alignment of the m-th range profile $(G_{\mathrm{m}}(\mathrm{n}))$ is calculated as

$$R_{\mathrm{m}}(\mathrm{n}) = \frac{\mathrm{m}-1}{\mathrm{m}} R_{\mathrm{m}-1}(\mathrm{n}) + \frac{1}{\mathrm{m}} |\widetilde{G}_{\mathrm{m}-1}(\mathrm{n})|, \tag{15}$$

where $R_{\mathrm{m}-1}(\mathrm{n})$ is the reference envelope for the $(\mathrm{m}-1)$-th range profile, $\widetilde{G}_{\mathrm{m}-1}(\mathrm{n})$ is the aligned $(\mathrm{m}-1)$-th range profile and n is the number of the range cell.

The shift, $\hat{n}_0$, between the reference envelope $R_{\mathrm{m}}(\mathrm{n})$ and the m-th range profile $G_{\mathrm{m}}(\mathrm{n})$ is obtained by maximizing the correlation between the absolute values of $R_{\mathrm{m}}(\mathrm{n})$ and a shifted version of $G_{\mathrm{m}}(\mathrm{n})$:

$$\hat{n}_0 = \arg\max_{n_0} \left[\sum_{\mathrm{n}} |R_{\mathrm{m}}(\mathrm{n})| \cdot |G_{\mathrm{m}}(\mathrm{n} - n_0)| \right] \tag{16}$$

This extension of the envelope correlation method is deeply explained in [11].

Firstly, the proposed algorithm is verified and compared for simulated data. The data were generated according to the data model in section II and the chosen scenario is the bi-dimensional one shown in Fig. 4. The simulation parameters are detailed in Table I.

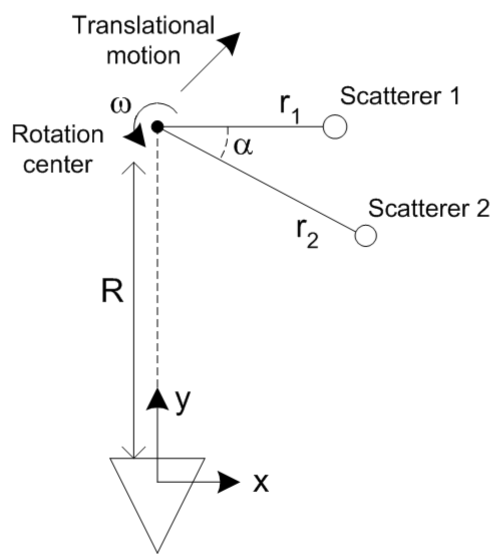

Fig. 4. Bi-dimensional scenario for simulated data

TABLE I
SIMULATION PARAMETERS

Angular rotation rate (ω)	0.2 rad/s	α	45°
Translational speed (**x** direction)	10 m/s	R	7000 m
Translational speed (**y** direction)	10 m/s	r_1, r_2	5 m
Translational acceleration (a_{e})	0 m/s^2	PRF	500 Hz
Number of range profiles	300	Δf	1 GHz
Sampling rate	40 MHz	T_{m}	2 ms
FFT points (down-range)	8192	f_0	28.5 GHz

Fig. 5 shows the ISAR images obtained using PPP, PGA and the proposed technique. We can see the MTRC associated with the scatterer 2, whose cause is the target rotational motion.

In order to make comparisons, as image focusing indicators, we use the peak value, the contrast and the entropy, whose expressions are given in (17), (18) and (19), respectively,

$$P.V. = 20 \cdot \log \left[\max_{\mathrm{i,j}} \left(|\mathbf{I}_{\mathrm{i,j}}| \right) \right], \tag{17}$$

$$C = \frac{\sqrt{A\{[|\mathbf{I}_{\mathrm{i,j}}|^2 - A\left(|\mathbf{I}_{\mathrm{i,j}}|^2\right)]^2\}}}{A\left(|\mathbf{I}_{\mathrm{i,j}}|^2\right)}, \tag{18}$$

$$E = -\sum_{\mathrm{i}} \sum_{\mathrm{j}} \bar{\mathbf{I}}_{\mathrm{i,j}} \cdot \ln \bar{\mathbf{I}}_{\mathrm{i,j}}, \tag{19}$$

where $\mathbf{I}_{\mathrm{i,j}}$ is the complex ISAR image, i and j are the spatial coordinates, the operator $A(\cdot)$ indicates spatial mean and $\bar{\mathbf{I}}_{\mathrm{i,j}}$ is the power normalized image, given by the expression

$$\bar{\mathbf{I}}_{\mathrm{i,j}} = \frac{|\mathbf{I}_{\mathrm{i,j}}|^2}{\sum_{\mathrm{i}} \sum_{\mathrm{j}} |\mathbf{I}_{\mathrm{i,j}}|^2}. \tag{20}$$

Better focusing means greater peak value, greater contrast and lower entropy. However, a high value of the peak does not guarantee a good focus of the whole image, but of a local area. Table II reports these values for the three images obtained with the simulated data.

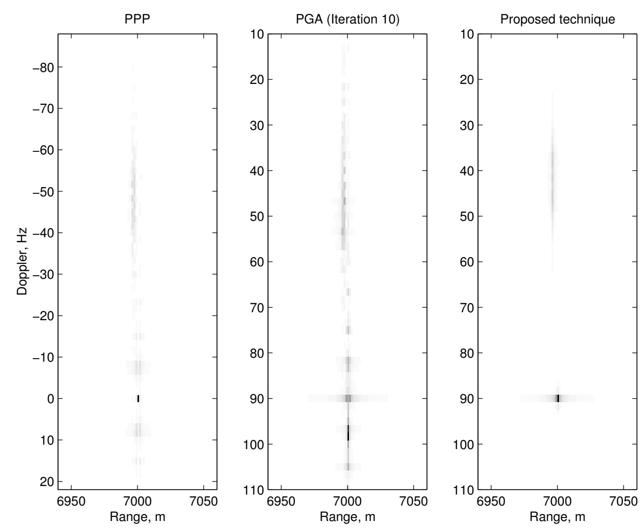

Fig. 5. ISAR images for simulated data

TABLE II
FOCUSING INDICATORS FOR SIMULATED DATA

	PPP	PGA	Proposed technique
Peak value (dB)	126.7	122.4	126.4
Contrast	11.99	13.85	24.62
Entropy	2.64	3.9	2.13

The algorithm has also been run for real data, captured by a high range resolution millimeter-wave radar [15]. The data corresponds to a ship. The PRF is 500 Hz, Δf is 1 GHz, T_{m} is 2 ms and the carrier is 28.5 GHz. Fig. 6 shows umbralized ISAR images obtained using PPP, PGA and the proposed technique. A high zoomed photo of the ship at the moment of capturing the data is shown in the upper right corner of Fig. 6. The focusing indicators are shown in Table III.

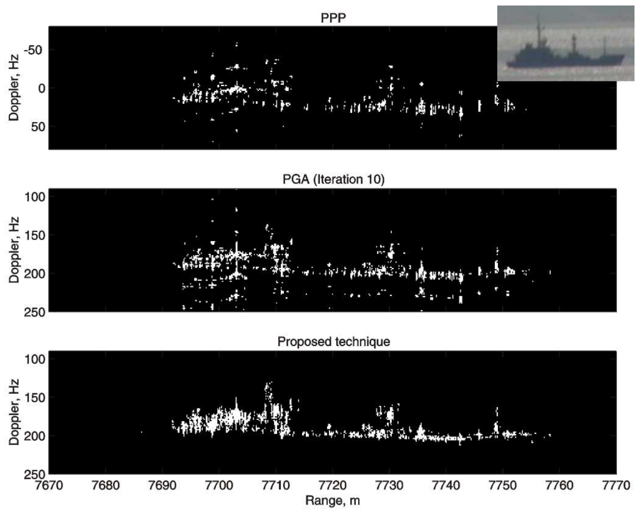

Fig. 6. ISAR images for real data

TABLE III

FOCUSING INDICATORS FOR REAL DATA

	PPP	PGA	Proposed technique
Peak value (dB)	70.9	68.2	67.2
Contrast	3.03	2.90	3.82
Entropy	7.30	7.66	7.05

The contrast and entropy values indicate a better focusing with the proposed technique. The image visual quality [12] confirms also this fact. Fig. 7 shows the umbralized ISAR image of the ship without using any translational motion compensation technique. Blurring artifacts exist in range and cross range. It is obvious that the translational motion must be compensated.

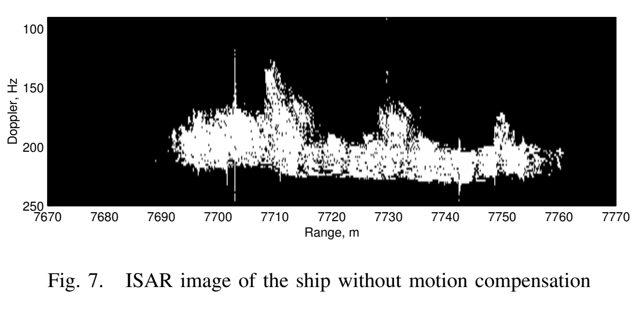

Fig. 7. ISAR image of the ship without motion compensation

The main drawback of the proposed new method is a large computational time, because of the shift-and-convolution algorithm. Nevertheless, a suitable DSP implementation could improve the time performance.

V. CONCLUSIONS

This paper presents a novel method for translational motion compensation in ISAR. Simulated data and real data from a high range resolution millimeter-wave LFMCW radar have been used to confirm the effectiveness of the proposed technique. The results have been compared with PPP and PGA (for the phase adjustment stage) and an extension of the envelope correlation method (for the range-bin alignment stage).

ACKNOWLEDGMENT

This work was supported by the Projects TIC02-04569-C02-01 and TIC02-02657-C02-01 of the National Board of Scientific and Technology Research.

REFERENCES

[1] Chen, C.C., Andrews, H.C., *Target Motion Induced Radar Imaging*, IEEE Transactions on Aerospace and Electronic Systems, Vol. 16, No. 1, pp. 2-14, 1980.
[2] Ausherman, D.A., Kozoma, A., Walker, J.L., Jones, H.M., Poggio, E.C., *Developments in Radar Imaging*, IEEE Transactions on Aerospace and Electronic Systems, Vol. 20, pp. 363-400, July 1984.
[3] Bao, Z., Sun, C., Xing, M., *Time-frequency approaches to ISAR imaging of maneuvering targets and their limitations*, IEEE Transactions on Aerospace and Electronic Systems, Vol. 37, No. 3, pp. 1091-1099, July 2001.
[4] Walker, J.L., *Range-Doppler Imaging of Rotating Objects*, IEEE Transactions on Aerospace and Electronic Systems, AES-16, pp. 23-52, Jan. 1980.
[5] Delisle, G.Y., Wu, H., *Moving target imaging and trajectory computation*, IEEE Transactions on Aerospace and Electronic Systems, Vol. 30, No. 3, pp. 887-889, July 1994.
[6] Wang, G., Bao, Z., *The minimum entropy criterion of range alignment in ISAR motion compensation*, Radar 97 (Conf. Publi. No. 449), 14-16 Oct. 1997, pp. 236-239.
[7] Sauer, T., Schroth, A., *Robust range alignment algorithm via Hough transform in an ISAR imaging system*, IEEE Transactions on Aerospace and Electronic Systems, Vol. 31, No. 3, pp. 1173-1177, July 1995.
[8] Wang, J., Kasilingam, D., *Global Range Alignment for ISAR*, IEEE Transactions on Aerospace and Electronic Systems, Vol. 39, No. 1, pp. 351-357, January 2003.
[9] Steinberg, B.D., *Microwave Imaging of Aircraft*, Proceedings of the IEEE, Vol. 76, No. 12, pp. 1578-1592, 1988.
[10] Wahl, D.E., Eichel, P.H., Ghiglia, D.C., Jakowatz, C.V., Jr., *Phase gradient autofocus - A robust tool for high resolution SAR phase correction*, IEEE Transactions on Aerospace and Electronic Systems, Vol. 30, No. 3, pp. 827-835. July 1994.
[11] Xi, L., Guosui, L., Ni, J., *Autofocusing of ISAR Images based on Entropy Minimization*, IEEE Transactions on Aerospace and Electronic Systems, Vol. 35, No. 4, pp. 1240-1252, October 1999.
[12] Martorella, M., Berizzi, F., Haywood, B., *Contrast maximisation based technique for 2-D ISAR autofocusing*, IEE Proceedings on Radar, Sonar and Navigation, Vol. 152, No. 4, pp. 253-262, August 2005.
[13] Carrara, W.G., Goodman, R.S., Majewski, R.M., *Spotlight synthetic aperture radar: Signal processing algorithms*, Artech House, Boston-London, 1995.
[14] Pérez-Martínez, F., García-Fominaya, J., Calvo-Gallego, J., *A Shift-and-Convolution Technique for High-Resolution Radar Images*, IEEE Sensors Journal, Vol. 5, No. 5, pp. 1090-1098, October 2005.
[15] Blanco-del-Campo, A., Asensio-López, A., Dorta-Naranjo, B.P., Gismero-Menoyo, J., Ramírez-Morán, D., Carmona-Duarte, C., Jiménez-Martín, J.L., *Millimeter-wave radar demonstrator for high resolution imaging*, First European Radar Conference, 2004. EURAD 2004. 11-15 October 2004, pp. 65-68.